3DMambalPF: A State Space Model for Iterative Point Cloud Filtering via Differentiable Rendering

Qingyuan Zhou zhouqy23@m.fudan.edu.cn School of Computer Science, Fudan University Shanghai, China

Jingyi Xu jyxu22@m.fudan.edu.cn School of Computer Science, Fudan University Shanghai, China Weidong Yang*
wdyang@fudan.edu.cn
School of Computer Science, Fudan
University
Shanghai, China

Rui Zhang 22210240379@m.fudan.edu.cn School of Computer Science, Fudan University Shanghai, China Ben Fei*
bfei21@m.fudan.edu.cn
School of Computer Science, Fudan
University
Shanghai, China

Keyi Liu 23210240242@m.fudan.edu.cn School of Computer Science, Fudan University Shanghai, China

Yeqi Luo 23212010018@m.fudan.edu.cn School of Computer Science, Fudan University Shanghai, China

ABSTRACT

Noise is an inevitable aspect of point cloud acquisition, necessitating filtering as a fundamental task within the realm of 3D vision. Existing learning-based filtering methods have shown promising capabilities on small-scale synthetic or real-world datasets. Nonetheless, the effectiveness of these methods is constrained when dealing with a substantial quantity of point clouds. This limitation primarily stems from their limited denoising capabilities for large-scale point clouds and their inclination to generate noisy outliers after denoising. The recent introduction of State Space Models (SSMs) for long sequence modeling in Natural Language Processing (NLP) presents a promising solution for handling large-scale data. Encouraged by iterative point cloud filtering methods, we introduce 3DMambaIPF, firstly incorporating Mamba (Selective SSM) architecture to sequentially handle extensive point clouds from large scenes, capitalizing on its strengths in selective input processing and long sequence modeling capabilities. Additionally, we integrate a robust and fast differentiable rendering loss to constrain the noisy points around the surface. In contrast to previous methodologies, this differentiable rendering loss enhances the visual realism of denoised geometric structures and aligns point cloud boundaries more closely with those observed in real-world objects. Extensive evaluations on datasets comprising small-scale synthetic and realworld models (typically with up to 50K points) demonstrate that our method achieves state-of-the-art results. Moreover, we showcase the superior scalability and efficiency of our method on large-scale models with about 500K points, where the majority of the existing learning-based denoising methods are unable to handle.

KEYWORDS

Point cloud filtering, denoising, state space model, differentiable rendering

yhe@ntu.edu.sg School of Computer Science and Engineering, Nanyang Technological

Ying He

University, Singapore

1 INTRODUCTION

Point clouds, assemblies of numerous three-dimensional points denoting spatial positions, play a crucial role in representing scenes across multimedia and computer vision (CV) domains. Nevertheless, as point clouds from real-world environments are captured by devices such as LiDAR, depth cameras, or 3D scanners, noises are inevitably introduced during the scanning process [11]. The presence of these noises undermines the required data consistency and accuracy in the application scenarios of point clouds, making filtering of point clouds a fundamental task within the realm of 3D vision [9, 10].

Due to the importance of point cloud filtering, numerous methods have been dedicated to improving the capabilities. Traditional point cloud filtering methods rely on expert priors, but they are limited by the accuracy of these priors and are not suitable for complex and sparse point clouds. In recent years, deep learningbased point cloud filtering methods have emerged prominently. These methods commonly employ iterative modules that consist of stacked encoder-decoder pairs. Such architectures leverage the output of the previous module as the input for the subsequent module, thereby demonstrating superior performance. For instance, Score-Denoise [36] utilizes gradient ascent techniques and introduces an iterative point-moving method based on estimated scores. IterativePFN [7] employs iterative modules and adaptive loss functions to iteratively and progressively refine noisy points toward adaptive ground truth (GT), yielding promising results on both synthetic and real-world datasets.

However, these point cloud filtering methods are only applicable to small-scale scenes and not suitable for denoising large-scale scenes. It is found experimentally that some denoising methods exhibit inadequate filtering capabilities when applied to large-scale point clouds. Furthermore, previous works only have demonstrated satisfactory performance solely in low-noise environments, but they

^{*}Corresponding author.

are limited to handling details in high-noise environments. This limitation is particularly evident in the generation of unrealistic boundaries, as well as a lack of appropriate constraints. Consequently, the main challenges are twofold: (i) denoising for large-scale point clouds or complex geometries, (ii) denoising for high-noise environments.

Recently, State Space Models (SSMs), particularly structured SSMs (S4) [15], have shown great promise in Natural Language Processing (NLP) [34]. Built upon the S4 framework, Mamba [13] exhibits outstanding performance across many tasks in NLP and 2D CV [18, 40, 51, 58]. These achievements of Mamba can be ascribed to the linear computational complexity and its proficient long-range context learning capabilities on long sequences. Furthermore, the utilization of time-varying parameters and a hardware-aware algorithm by Mamba represents significant advancements in sequence modeling.

Considering the aforementioned challenges in point cloud filtering and the strength of Mamba for long sequence modeling, we propose 3DMambaIPF, a novel Iterative Point Clouds Filtering model utilizing the Mamba module with point rendering techniques. Specifically, 3DMambaIPF is composed of multiple iterations of Mamba-Denoise Modules, each comprising a pair of Mamba encoders and decoders. Initially, the input point cloud is divided into patches, within which a graph structure is generated based on points and their neighbors to extract position features. In the Mamba-Encoder, the Dynamic EdgeConv module encodes positional features with MLPs, which are then inputted into a Mamba module to select and generate position-dependent features from sequential inputs. The Mamba-Decoder is responsible for upsampling features into point cloud patches. During the training process, a novel rendering loss is introduced leveraging a differential point rendering technique, and the loss is computed by the disparities of rendered images of filtered point cloud and GT. Subsequently, an adaptive GT altering throughout the iterations is introduced, gradually transitioning from an initially noise-added state to the true GT. Following the completion of all iterations, a patch-stitching method is employed to reconstruct the denoised point cloud from the patches. Experimentally, 3DMambaIPF is trained using PU-Net [53] dataset and achieves state-of-the-art results compared to off-the-shelf methods. 3DMabaIPF is also able to well generalize to high-noise point clouds from the Stanford 3D Scanning Repository [6, 26] for synthetic objects with complex geometries. Moreover, 3DMambaIPF outperforms baseline methods in terms of visual perceptions on real-world scene datasets. In summary, our specific contributions are as follows:

- Mamba module is integrated into the iterative filtering module, enabling modeling and filtering of long-sequence point cloud features, thereby achieving more accurate and rapid modeling of large-scale point clouds.
- A novel, differentiable point rendering loss is integrated into 3DMambaIPF, supplanting the distance-based loss functions employed in previous methods. This enhancement endows 3DMambaIPF with the ability to handle edge denoising and makes the denoising results more realistic.
- 3DMambaIPF surpasses baseline methods by achieving stateof-the-art results on both synthetic and real-world scene

datasets, while demonstrating excellent performance even on high-noise large-scale synthetic dataset.

2 RELATED WORK

2.1 Point Cloud Filtering Methods

Traditional point cloud filtering methods can be categorized into several main classes. Geometry-based approaches [1, 2, 5, 22, 31, 38] involve projecting point clouds onto a surface and utilize geometric features, such as parameters derived from local surface fitting and normal estimation, to describe the shape and structure of the point cloud. Statistical-based methods [3, 28, 46, 48, 49, 55] employ techniques such as sparse reconstruction, density estimation and clustering analysis. Moreover, graph-based methods [12, 20, 21] utilize graph structures to represent the relationships between points. These methods leverage graph filters and graph signal processing techniques to denoise point clouds effectively. By modeling point clouds as graphs, where each point is a node and connections between points represent geometric relationships, graph-based methods can exploit the inherent connectivity and structure of the data for noise reduction. Nonetheless, traditional methods consistently prove inadequate in effectively denoising point clouds with large-scale and complex geometries.

Deep Learning-based point cloud filtering methods are undergoing significant development to address the limitations of traditional approaches. The well-known PCN (PointCleanNet) [44] model is based on PCPNet [17] and focuses on removing outliers and reducing noise in unordered point clouds. However, due to PCN's denoising being performed point-wise rather than patchwise, its efficiency is relatively low. PD-Flow [37] learns the distribution of noisy point sets and achieves denoising through noise disentanglement. However, the number of iterations needed for PD-Flow varies depending on the level of noise to achieve optimal results. GPDNet [43] employs graph-convolutional layers to dynamically build neighborhood graphs and utilizes the similarity of high-dimensional feature representations to construct intricate feature hierarchies. ScoreDenoise [36] leverages the distribution model and score estimation from noisy point clouds. Pointfilter [56] employs an encoder-decoder architecture, where points and their neighbors are taken as input for point-wise learning. It generates a displacement vector to accomplish denoising while preserving sharp features. IterativePFN [7] leverages iterative filtering modules and adaptive GT progressively yet swiftly converges noisy points onto clean surfaces, achieving superior performance. Current point cloud filtering methods are primarily designed for small-scale scenes (about 50K points) and struggle to effectively denoise point clouds with dense noise, particularly those far from clean surfaces, especially in large-scale scenes (about 500K points). Furthermore, existing methods [56] demonstrate limited effectiveness in filtering the edges of point clouds and capturing fine-grained characteristics. Considering these challenges, our work aims to introduce a model tailored for large-scale scenes characterized by high-density noise and robust denoising capabilities at point cloud edges.

2.2 SSM-based Methods

SSMs provide a robust mathematical framework rooted in control theory and are increasingly applied in fields such as NLP and CV

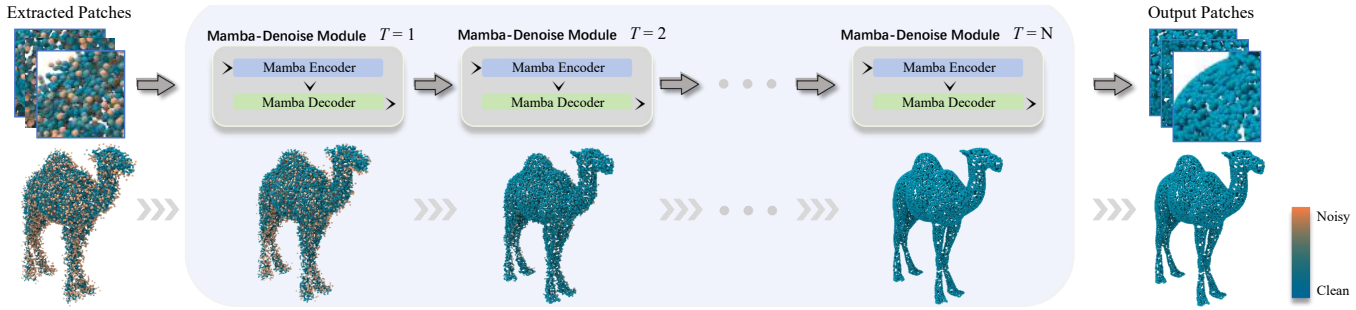


Figure 1: Overview of 3DMambaIPF. An Encoder-Decoder-based model built on Mamba named Mamba-Denoise Module is introduced for iterative filtering. The input noisy point cloud is partitioned into patches and fed into the iterative Mamba-Denoise Module. Upon completion of the iterations, clean point cloud patches are produced as output.



Figure 2: A Gaussian noise with a variable standard deviation is added to the GT to generate the adaptive GT. As the standard deviation gradually decreases, the adaptive GT approaches the GT with each iteration. Eventually, the GT no longer changes in the final iteration.

to model complex temporal dynamics within dynamic systems. This novel modeling approach addresses the challenge of handling long sequences, a difficulty encountered by both Transformers and RNNs. By mitigating the quadratic computational complexity of Transformers and addressing the forgetting issue of RNNs, SSMs prove highly efficient in capturing temporal dependencies within sequential data.

One noteworthy advancement in SSMs is the introduction of the HiPPO [14], which simplifies input sequence modeling by compressing inputs into a dynamic, polynomial-based representation. However, despite this innovative approach, high computational and memory footprint limit the applicability as a general sequence modeling solution [16], failing to fully address the bottleneck issues inherent in SSMs. To this end, the S4 [15] presents a novel parameterization technique. By integrating a low-rank structured correction, S4 achieves stable diagonalization, significantly enhancing computational efficiency through simplified Cauchy kernel operations.

Significant advancements have been made in the Mamba framework [13], which integrates selective SSMs into a simplified architecture. This integration allows Mamba to achieve rapid inference, linear scalability in sequence length, and state-of-the-art performance across multiple modalities, while also enhancing the selectivity of state representation. These advancements collectively demonstrate the ongoing evolution of SSMs and their increasing significance in modeling temporal dynamics across diverse domains. Methods based on Mamba have achieved state-of-the-art results in various fields, including large language models [18, 51], medical image analysis [23, 30, 54], and 3D point cloud perception [29, 32, 57]. Taking Consideration of the advantages of Mamba in modeling long sequences, we introduce Mamba in our work to address point cloud modeling problems in large-scale scenes.

2.3 Differentiable Rendering Techniques

Rendering techniques encompass algorithms employed to transform three-dimensional models into two-dimensional images. The differentiable rendering methods are designed for introduction into deep learning, facilitating 3D reconstruction through error backpropagation. Current differentiable rendering methods can be categorized into four types based on their geometric representations: point-based [8, 24, 25, 41, 52], triangle mesh-based [19, 27, 33], implicit function-based[4, 50], and volume-based[39, 45]. In this paper, we utilize an efficient differentiable point-based rendering method [24] to render both the filtered and ground-truth point clouds during training to generate the view loss, which is then propagated backward to adjust the network parameters.

3 PRELIMINARIES

Structured State Space Models are two-stage sequence-to-sequence models that map the input $x(t) \in \mathbb{R}^L$ to output $y(t) \in \mathbb{R}^L$. Specifically, the SSM process can be described as follows:

$$h'(t) = \mathbf{A}h(t) + \mathbf{B}x(t),$$

$$y(t) = \mathbf{C}h(t),$$
 (1)

where $h(t) \in \mathbb{R}^N$ represents the latent state, and $h'(t) \in \mathbb{R}^N$ is the derivative of h(t). $\mathbf{A} \in \mathbb{R}^{N \times N}$, $\mathbf{B} \in \mathbb{R}^{N \times 1}$, $\mathbf{C} \in \mathbb{R}^{1 \times N}$ are the parameters. The first stage of S4 discretizes the parameter \mathbf{A} , \mathbf{B} into $\bar{\mathbf{A}}$, $\bar{\mathbf{B}}$ with a parameter Δ :

$$\bar{\mathbf{A}} = \exp(\Delta \mathbf{A}),$$

$$\bar{\mathbf{B}} = (\Delta \mathbf{A})^{-1} (\exp(\Delta \mathbf{A}) - I) \cdot \Delta \mathbf{B}.$$
(2)

After discretizing, the second stage is to calculate recursively:

$$h_t = \bar{\mathbf{A}}h_{t-1} + \bar{\mathbf{B}}x_t,$$

$$y_t = \mathbf{C}h_t,$$
(3)

with the convolution formula:

$$\bar{\mathbf{K}} = (\mathbf{C}\bar{\mathbf{B}}, \mathbf{C}\bar{\mathbf{A}}\bar{\mathbf{B}}, ..., \mathbf{C}\bar{\mathbf{A}}^{k}\bar{\mathbf{B}}, ...),$$

$$y = x * \bar{\mathbf{K}}.$$
(4)

Mamba, as mentioned in Section 2.2, employs recurrent scans coupled with a selection mechanism to regulate the passage of specific segments within the sequence into the latent states. Specifically, by making the SSM parameters functions of the input, Mamba addresses the weakness in dealing with discrete modalities, allowing the model to selectively propagate or forget information based on

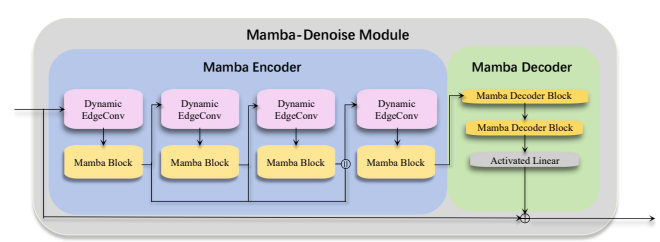


Figure 3: Recurrent Point Cloud Filtering of 3DMambaIPF. The Mamba Encoder comprises Dynamic EdgeConv modules and Mamba Blocks, while the Mamba Decoder consists of Mamba-Decoder Blocks and an Activated Linear module.

the current token. Simultaneously, Mamba has devised a hardware-aware parallel algorithm to operate in recursive mode, addressing the challenge of inefficient convolution operations. The structure diagram of a single Mamba block is illustrated in Figure 4, where the overall process can be viewed as a transition from $x_{t-1} \in \mathbb{R}^L$ to $x_t \in \mathbb{R}^L$:

$$x_{t}' = \text{DWConv}(\text{MLP}(\text{LN}(x_{t-1}))),$$

$$s_{t} = \text{MLP}(\text{LN}(\text{SSM}(\sigma(x_{t}'))) \times \sigma(\text{LN}(x_{t-1}))),$$

$$x_{t} = s_{t} + x_{t-1},$$
(5)

where DWC onv represents depth-wise convolution, LN represents layer normalization, σ denotes activation (SiLU here).

4 METHOD

4.1 Overview

In this section, building on top of IterativePFN [7], we will detailly introduce 3DMambaIPF which is the first Mamba framework for iteratively filtering 3D point clouds via differentiable point rendering. The recurrent point cloud filtering structure of the 3DMambaIPF model is depicted in Figure 1. 3DMambaIPF network consists of a cascade of Mamba encoders and Mamba decoders, with each pair referred to as a Mamba-Denoise Module. After receiving an extracted patch of the point cloud as input, a single Mamba-Denoise Module constructs a directed graph from the points within the patch. The directed graph is encoded into token sequences to extract features. The denoised point token sequences are then decoded, eliminating noise, and serve as the input for the next Mamba-Denoise Module. Subsequently, we will employ a differentiable 3D point rendering loss to refine the positions of noisy points. This will be achieved by comparing the rendered images from denoised point clouds with the GT. This process iterates until the final module is reached, after which the final output is a clean point cloud patch. The recurrent point cloud filtering method will be introduced in Section 4.2, the Mamba-Denoising encoder and decoder module will be introduced in Section 4.3. Section 4.4 will introduce differentiable point rendering techniques and backpropagation, while Section 4.5 will specifically describe loss function used in 3DMambaIPF.

4.2 Recurrent Point Cloud Filtering

Given a 3-dimensional clean point cloud, denoted as $X_c = \{x_{c1}, x_{c2}, ... x_{cn}\} \subseteq \mathbb{R}^3$, each point in X_c can be represented by three-dimensional coordinates $x_{ci} = (\alpha_i, \beta_i, \gamma_i)$. To prepare the point cloud as input for the network, the K-nearest neighbors (KNN)

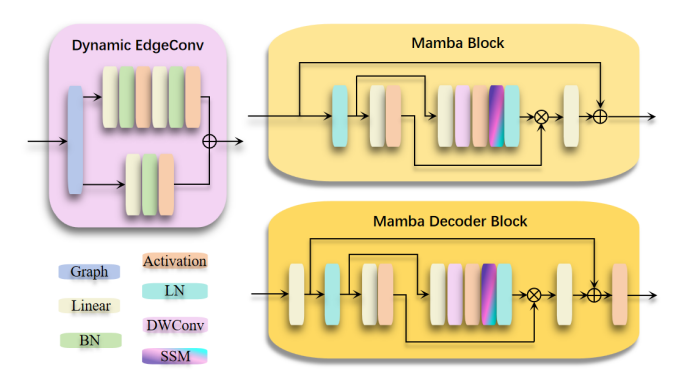


Figure 4: Detailed network architectures for Dynamic Edge-Conv, Mamba Block, and Mamba Decoder Block.

algorithm [42] is used to partition the point cloud into patches, and a directed graph is constructed within each patch. Considering a point cloud patch $X \subseteq \mathbb{K}^3$ which generated by KNN and a directed graph $\mathcal{G} = \{\mathcal{V}, \mathcal{E}\}$, where $\mathcal{V} = \{x_1, x_2, ... x_K\}$ and \mathcal{E} represents the edges between $x_i \in \mathcal{V}$ and its k-nearest neighbors.

In the recurrent point cloud filtering method, we follow IterativePFN [7] and introduce the adaptive GT, gradually pulling noisy points closer to the clean surface in each iteration process. As shown in Figure 2, GT is adaptive at each iteration, except for the last one. Specifically, to generate the noisy point cloud $X_n \subseteq \mathbb{R}^3$ as the adaptive GT, perturbed points are formed by adding Gaussian noise to X_c with a standard deviation σ between 0.5% and 2% of the radius of the bounding sphere. As the number of iterations increases, σ decreases continuously, eventually reaching 0 at the final iteration. During each iteration, we aim to minimize the loss function to bring x_i closer to its nearest neighbors in adaptive GT.

4.3 Mamba-Denoising Backbone

The Mamba-Denoising Backbone is the core component of 3DMambaIPF for recurrent point cloud filtering. As illustrated in Figure 3, the Mamba-Denoising backbone adopts an Encoder-Decoder structure. The encoder consists of four Dynamic EdgeConv modules and four corresponding Mamba Blocks respectively, while the decoder comprises a Mamba Decoder Block and a linear activation layer. The detailed network structure is illustrated in Figure 4.

The Dynamic EdgeConv module facilitates the conversion of input patches into a graph structure, subsequently processed through an MLP network to extract pertinent features. Initially, vertices undergo feature extraction via an MLP, capturing intrinsic characteristics. Subsequently, an additional MLP focuses on extracting positional features from vertices connected by edges to the target vertex, facilitating feature differentiation. This process culminates in concatenating the target vertex's features with the differences of features computed from all connected vertices, effectively deriving nuanced positional features within the patch. Following the feature extraction of the point cloud within the patch using MLPs, the resultant feature sequence is sent to the Mamba Encoder. This encoder selectively processes the input feature sequence and alters it into an output feature sequence. In the Decoder module, the Mamba Decoder Block selectively processes the input feature sequence to

reduce dimensionality, gradually reconstructing it into three dimensions. Linear activation is used to determine an output movement distance of a noisy point towards a clean surface after filtering. Distance values are then combined with a residual connection to the input patch, yielding the denoised point cloud patch.

4.4 Differentiable Rendering and Backpropagation

For enhanced filtering of the edges in noisy point clouds, a differentiable rendering method is devised in 3DMambaIPF, explicitly quantifying the level of noise and enabling backpropagation. To render the point clouds, 3D coordinates of the raw point cloud's are initially converted into the standard coordinate frame via a projective transformation aligned with the camera pose. Subsequently, each discretized point is expressed as scaled Gaussian densities, yielding the occupancy map, and making the backpropagation available. Through the introduction of a differentiable ray tracing operator, these occupancies are transformed into ray termination probabilities. Ultimately, the rendered image is generated by projecting the volume onto the plane.

As depicted in Figure 5, denoised point cloud and adaptive GT are utilized to produce K pairs of images with fixed camera poses using point rendering technique introduced above. These images are then used to calculate a rendering loss, which constitutes a part of the overall loss function. Since the entire rendering process is differentiable, 3DMambaIPF encourages the denoised point cloud to achieve improved geometric appearance, particularly at the boundaries, throughout the backpropagation process.

4.5 Loss Function

Our loss function comprises two components: reconstruction loss and rendering loss. The reconstruction loss aims to minimize the distance between each point in the noisy point cloud and its closest counterpart in the adaptive GT, thereby structurally denoising the point cloud. Specifically, it seeks to bring every point in the noisy point cloud closer to its corresponding (the nearest) point in the adaptive GT.

Due to the possibility of overlapping regions within each patch during patch partitioning, we introduce a patch stitching method [59]. This method weights input points based on the proximity of each point p_i to a reference point p_r with a Gaussian distribution. Specifically, the weight w_i for each p_i is calculated as Eq. 6:

$$w_i = \frac{\exp(-\|p_i - p_r\|^2 / 2r_s^2)}{\sum_i \exp(-\|p_i - p_r\|^2 / 2r_s^2)}.$$
 (6)

Taking reference from [7], the support radius r_s is set to r/3, where r is the patch radius. Then, the reconstruction loss at the t-th iteration can be defined as Eq. 7:

$$\mathcal{L}_{Recon}(t) = \sum_{\hat{p}_i \in \hat{\mathcal{P}}} w_i \min_{p_{ti} \in \mathcal{P}_t} \|p_{ti} - \hat{p}_i\|_2^2, \tag{7}$$

where $\hat{\mathcal{P}}$ denotes the predicted point cloud, \mathcal{P}_t denotes the adaptive GT at the t-th iteration, and p_i represents a point in point cloud \mathcal{P} .

On the other hand, the rendering loss focuses on visually aligning the noisy point cloud with the adaptive GT using differentiable rendering techniques. As calculated by Eq. 8, it primarily concentrates

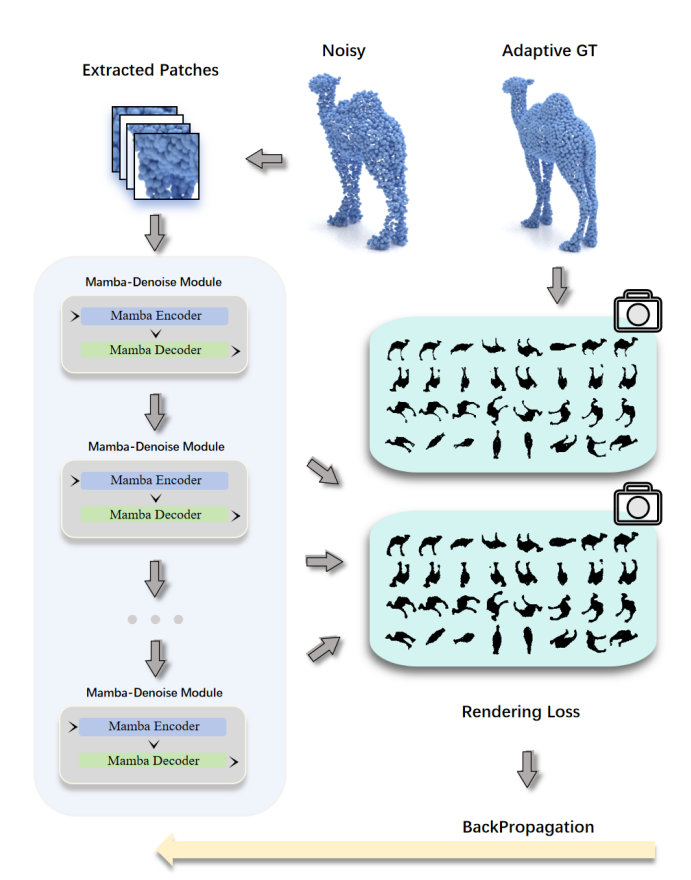


Figure 5: Diagram for rendering loss and backpropagation. on optimizing the boundary regions of the point cloud:

$$\mathcal{L}_{Render}(t) = \frac{1}{K} \sum_{i=1}^{K} |V_i(\mathcal{P}_t) - V_i(\hat{\mathcal{P}})|, \tag{8}$$

where $\hat{\mathcal{P}}$ denotes the predicted point cloud, \mathcal{P}_t denotes the adaptive GT at the t-th iteration, K is the quantity of rendered views, and V_i represents a rendered view in a specific camera position. Loss function of one iteration is a weighted combination of the reconstruction loss and the rendering loss, and the ultimate loss is obtained by aggregating loss contributions across iterations, which are summed up as Eq. 9:

$$\mathcal{L} = \sum_{t=1}^{T} (\mathcal{L}_{Recon}(t) + \alpha \mathcal{L}_{Render}(t)), \tag{9}$$

where T is number of iteration times, and weight α is 0.01 in experiments.

5 EXPERIMENTS

5.1 Datasets and Implementation

Datasets. Following previous works [7, 36, 37], 3DMambaIPF is trained with PU-Net [53] dataset. The training set consists of 40 sets of meshes, from which point clouds are generated at resolutions of 10K, 30K, and 50K, resulting in a total of 120 point clouds for training. To create noisy inputs, Gaussian noise is added to each point cloud with standard deviations of 0.5%, 1.0%, 1.5%, and 2% of the diagonal length of the object bounding box respectively. Similar

| | | | 10K p | oints | | 50K points | | | | | | | |
|-------------------|-------|----------|-------|----------|--------|------------|-------|----------|-------|----------|-------|-------|--|
| Method | 1% n | 1% noise | | 2% noise | | 2.5% noise | | 1% noise | | 2% noise | | noise | |
| | CD | P2M | CD | P2M | CD | P2M | CD | P2M | CD | P2M | CD | P2M | |
| Noisy | 36.90 | 16.03 | 79.39 | 47.72 | 105.02 | 70.03 | 18.69 | 12.82 | 50.48 | 41.36 | 72.49 | 62.03 | |
| PCN | 36.86 | 15.99 | 79.26 | 47.59 | 104.86 | 69.87 | 11.03 | 6.46 | 19.78 | 13.70 | 32.03 | 24.86 | |
| GPDNet | 23.10 | 7.14 | 42.84 | 18.55 | 58.37 | 30.66 | 10.49 | 6.35 | 32.88 | 25.03 | 50.85 | 41.34 | |
| DMRDenoise | 47.12 | 21.96 | 50.85 | 25.23 | 52.77 | 26.69 | 12.05 | 7.62 | 14.43 | 9.70 | 16.96 | 11.90 | |
| PDFlow | 21.26 | 6.74 | 32.46 | 13.24 | 36.27 | 17.02 | 6.51 | 4.16 | 12.70 | 9.21 | 18.74 | 14.26 | |
| ScoreDenoise | 25.22 | 7.54 | 36.83 | 13.80 | 42.32 | 19.04 | 7.16 | 4.00 | 12.89 | 8.33 | 14.45 | 9.58 | |
| Pointfilter | 24.61 | 7.30 | 35.34 | 11.55 | 40.99 | 15.05 | 7.58 | 4.32 | 9.07 | 5.07 | 10.99 | 6.29 | |
| IterativePFN | 20.55 | 5.01 | 30.43 | 8.43 | 33.53 | 10.46 | 6.05 | 3.02 | 8.03 | 4.36 | 10.15 | 5.88 | |
| 3DMambaIPF (Ours) | 19.89 | 4.77 | 29.95 | 8.03 | 32.62 | 9.92 | 5.89 | 2.91 | 7.55 | 4.05 | 9.28 | 5.31 | |

Table 1: Results on PU-Net Dataset. CD and P2M distances are multiplied by 10⁵.

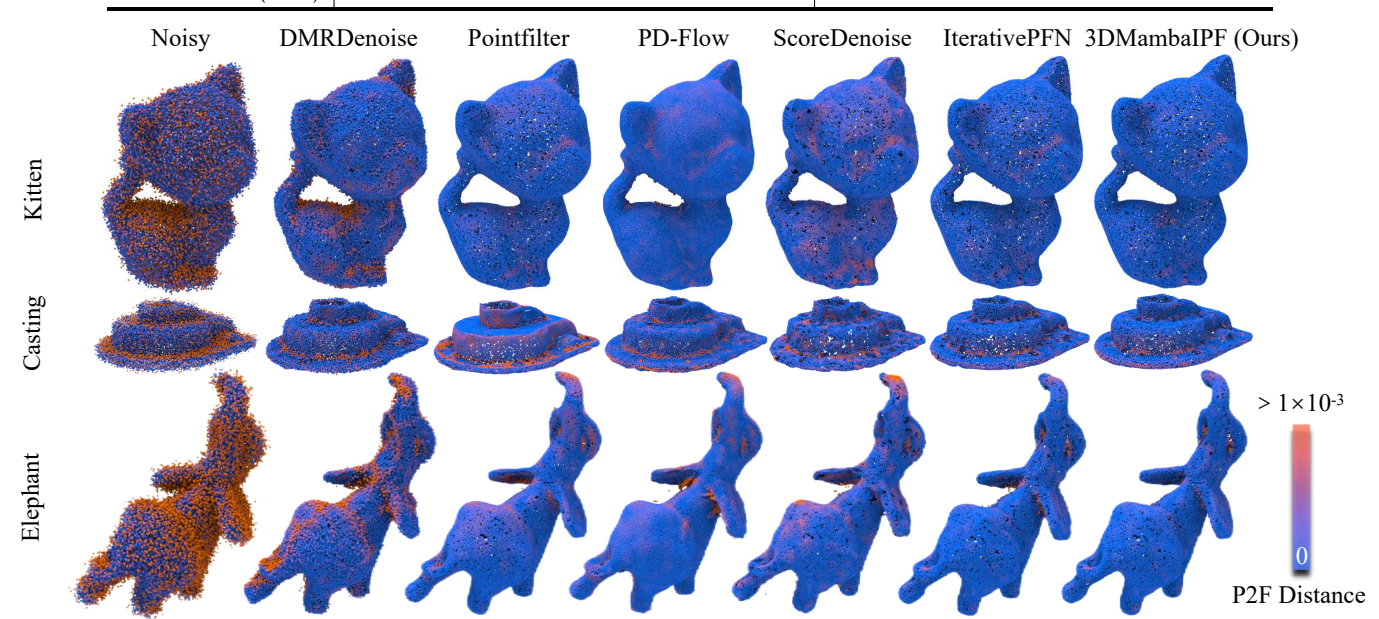


Figure 6: Visualization Comparisons on PU-Net Dataset of 50K points with 2.5% Gaussian deviation. The coloration of each point is determined by its point-wise P2F distance, with points exhibiting low P2F values (clean) depicted in blue, while those with high P2F values (noisy) are portrayed in red.

to IterativePFN [7], we conduct testing with 20 sets of meshes, generating point clouds at resolutions of 10K and 50K, resulting in a total of 40 point clouds.

Due to the limited number of points in PU-Net dataset, which contains a maximum of 50K points, Armadillo (about 173K points) and Dragon (about 438K points) from the Stanford 3D Scanning Repository [6, 26] are utilized to evaluate the filtering performance of large-scale synthetic objects. A higher degree of Gaussian noise is added to the Dragon point cloud, with a standard deviation of 5% of the diagonal length of the object bounding box. Simultaneously, a constraint term is introduced to ensure that the added noise is kept clear of the point cloud boundaries to a certain extent. Additionally, Paris-rue-Madame dataset [47], comprising authentic street scenes captured in Paris via a 3D mobile laser scanner, is employed in the experiments.

Implementation. The 3DMambaIPF network is trained on NVIDIA A100 GPUs with PyTorch 1.13.1 and CUDA 11.7. The network underwent 100 epochs of training on PU-Net dataset, employing the Adam optimizer with a learning rate of 1×10^{-4} . Comparative experiments are conducted with DMRDenoise [35], Pointfilter [56], PD-Flow [37], ScoreDenoise [36] and IterativePFN [7]. All experimental methods (including 3DMambaIPF) are tested on the NVIDIA GeForce RTX 3090 GPU for consistency across evaluations in this paper.

5.2 Evaluation metrics

Referring to many prior notable works, we utilize Chamfer Distance (CD) and Point-to-Mesh (P2M) Distance as the evaluation metrics for our study. Notably, CD is delineated in Eq. 10, encompassing the combined sum of two components: the average distances between each point in the predicted point cloud and its nearest point in the GT point cloud, and the average distances between each point

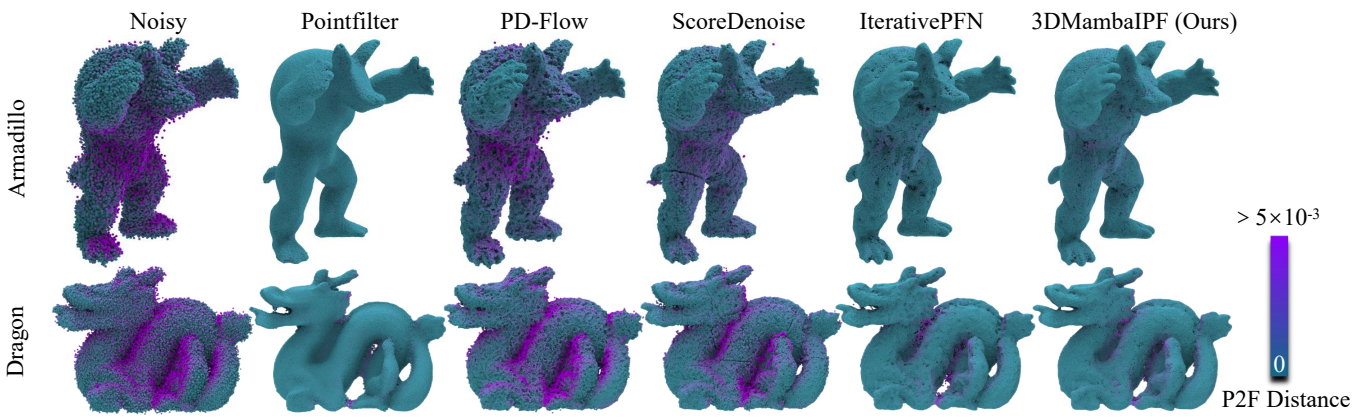


Figure 7: Visualization Comparisons on large-scale models from the Stanford 3D Scanning Repository with 5% Gaussian deviation. Coloration of each point is determined by its point-wise P2F distance, with points exhibiting low P2F values (clean) depicted in green, while those with high P2F values (noisy) are portrayed in purple.

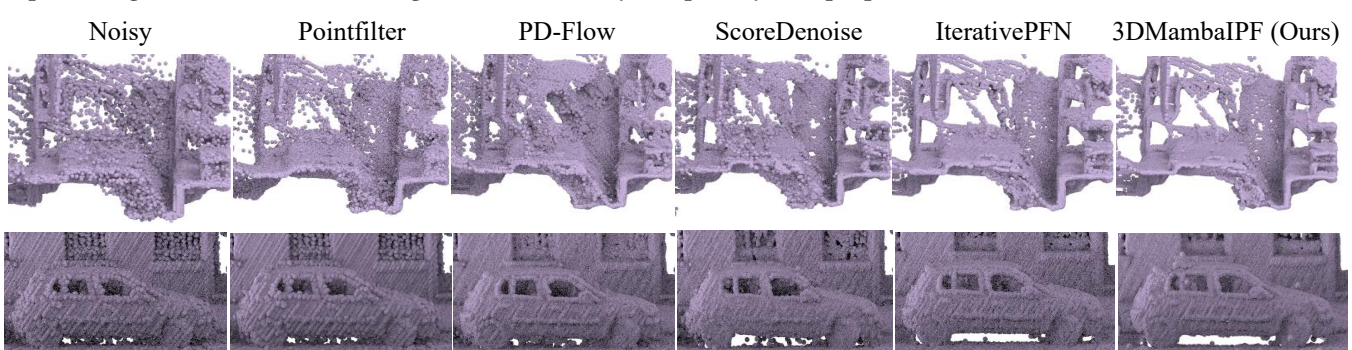


Figure 8: Visualization Comparisons on Paris-rue-Madame dataset.

Table 2: Ablation results of loss function on PU-Net Dataset. CD and P2M distances are multiplied by 10⁵.

| | | | 10K p | oints | | 50K points | | | | | | |
|--|-----------------------|---------------------|-----------------------|---------------------|-----------------------|----------------------|---------------------|---------------------|---------------------|---------------------|---------------------|---------------------|
| Method | 1% noise | | 2% noise | | 2.5% noise | | 1% noise | | 2% noise | | 2.5% noise | |
| | CD | P2M | CD | P2M | CD | P2M | CD | P2M | CD | P2M | CD | P2M |
| IterativePFN | 20.56 | 5.01 | 30.43 | 8.45 | 33.52 | 10.45 | 6.05 | 3.02 | 8.03 | 4.36 | 10.15 | 5.88 |
| 3DMambaIPF (without view loss) 3DMambaIPF (with view loss) | 20.02 19.89 | 4.80 4.77 | 30.19 29.95 | 8.13 8.03 | 32.97 32.62 | 10.05 9.92 | 5.94 5.89 | 2.92 2.91 | 7.70 7.55 | 4.14 4.05 | 9.41 9.28 | 5.37 5.31 |

in the GT point cloud and its nearest point in the predicted point cloud.

as F2P), as represented by Eq. 11.

$$\mathcal{L}_{P2M}(\hat{\mathcal{P}}, \mathcal{M}) = \mathcal{L}_{P2F}(\hat{\mathcal{P}}, \mathcal{M}) + \mathcal{L}_{F2P}(\hat{\mathcal{P}}, \mathcal{M}),$$

$$\mathcal{L}_{P2F}(\hat{\mathcal{P}}, \mathcal{M}) = \frac{1}{|\hat{\mathcal{P}}|} \sum_{\hat{p} \in \hat{\mathcal{P}}} \min_{f \in \mathcal{M}} d(\hat{p}, f),$$

$$\mathcal{L}_{F2P}(\hat{\mathcal{P}}, \mathcal{M}) = \frac{1}{|\mathcal{M}|} \sum_{f \in \mathcal{M}} \min_{\hat{p} \in \hat{\mathcal{P}}} d(\hat{p}, f),$$
(11)

 $\mathcal{L}_{CD}(\hat{\mathcal{P}}, \mathcal{P}) = \frac{1}{|\hat{\mathcal{P}}|} \sum_{\hat{p} \in \hat{\mathcal{P}}} \min_{p \in \mathcal{P}} \|\hat{p} - p\| + \frac{1}{|\mathcal{P}|} \sum_{p \in \mathcal{P}} \min_{\hat{p} \in \hat{\mathcal{P}}} \|p - \hat{p}\|,$ $\tag{1}$

where $\hat{\mathcal{P}}$ represents the predicted point cloud, \mathcal{P} represents the GT point cloud, $|\mathcal{P}|$ signifies the number of points in \mathcal{P} , and $||\cdot||$ denotes L2 norm. Similarly, the P2M Distance consists of two components: the average distance from each point in the predicted point cloud to the nearest face in the GT point cloud (referred to as P2F), and the sum of the average distances from each face in the GT point cloud to the nearest point in the predicted point cloud (referred to

where $\hat{\mathcal{P}}$ represents the predicted point cloud, \mathcal{M} represents the mesh of GT point cloud, $|\mathcal{P}|$ signifies the number of points in \mathcal{P} , $|\mathcal{M}|$ signifies the number of faces in \mathcal{M} , and d(p,f) denotes square distance from point p to face f. Please note that due to the typically unequal quantities of faces and points, point-wise calculation of P2M distance is unreasonable. In the visualization of denoising results in Section 5.3 and Section 5.4, we utilize the point-wise P2F distance from Eq. 11 to visualize the denoised point cloud results.

Table 3: Ablation results of views in point rendering on PU-Net Dataset. CD and P2M distances are multiplied by 10⁵.

| | Rendered | | | 10K p | oints | | 50K points | | | | | | |
|--------------|----------|-------|------|-------|-------|-------|------------|------|-------|------|-------|-------|-------|
| Method | Views | 1% n | oise | 2% n | oise | 2.5% | noise | 1% r | noise | 2% r | noise | 2.5% | noise |
| | views | CD | P2M | CD | P2M | CD | P2M | CD | P2M | CD | P2M | CD | P2M |
| IterativePFN | / | 20.56 | 5.01 | 30.43 | 8.45 | 33.52 | 10.45 | 6.05 | 3.02 | 8.03 | 4.36 | 10.15 | 5.88 |
| 3DMambaIPF | 8 | 20.36 | 4.96 | 30.73 | 8.48 | 34.35 | 10.96 | 6.04 | 2.99 | 8.06 | 4.36 | 10.39 | 6.05 |
| 3DMambaIPF | 16 | 20.29 | 4.97 | 30.35 | 8.24 | 33.08 | 10.21 | 6.21 | 3.14 | 7.87 | 4.29 | 9.63 | 5.60 |
| 3DMambaIPF | 24 | 19.96 | 4.82 | 30.26 | 8.14 | 32.85 | 9.95 | 5.96 | 2.97 | 7.81 | 4.26 | 9.56 | 5.53 |
| 3DMambaIPF | 32 | 19.89 | 4.77 | 29.95 | 8.03 | 32.62 | 9.92 | 5.89 | 2.91 | 7.55 | 4.05 | 9.28 | 5.31 |

Table 4: Ablation results of Mamba layers on PU-Net Dataset. CD and P2M distances are multiplied by 10⁵.

| Mo | Mamba | | | 10K p | oints | | 50K points | | | | | | |
|--------------|--------|-------|------|-------|-------|-------|------------|------|-------|-------|------|-------|-------|
| Method | Lavers | 1% n | oise | 2% n | oise | 2.5% | noise | 1% r | noise | 2% n | oise | 2.5% | noise |
| | Layers | CD | P2M | CD | P2M | CD | P2M | CD | P2M | CD | P2M | CD | P2M |
| IterativePFN | / | 20.56 | 5.01 | 30.43 | 8.45 | 33.52 | 10.45 | 6.05 | 3.02 | 8.03 | 4.36 | 10.15 | 5.88 |
| 3DMambaIPF | 1 | 23.35 | 6.76 | 33.24 | 10.91 | 36.42 | 13.17 | 8.15 | 4.71 | 10.82 | 6.53 | 13.23 | 8.20 |
| 3DMambaIPF | 3 | 20.24 | 5.02 | 30.59 | 8.61 | 33.44 | 10.60 | 6.12 | 3.09 | 8.05 | 4.43 | 9.58 | 5.54 |
| 3DMambaIPF | 6 | 19.89 | 4.77 | 29.95 | 8.03 | 32.62 | 9.92 | 5.89 | 2.91 | 7.55 | 4.05 | 9.28 | 5.31 |
| 3DMambaIPF | 9 | 20.55 | 5.11 | 30.77 | 8.59 | 33.82 | 10.70 | 6.15 | 3.08 | 8.01 | 4.38 | 9.89 | 5.74 |
| 3DMambaIPF | 12 | 20.48 | 5.05 | 30.83 | 8.80 | 33.92 | 10.98 | 6.12 | 3.07 | 8.09 | 4.42 | 9.85 | 5.67 |

Table 5: Ablation results of patch size on PU-Net Dataset. CD and P2M distances are multiplied by 10⁵.

| Method | Patch | 1% n | oise | 10K points 2% noise | | 2.5% noise | | 1% noise | | 50K points 2% noise | | 2.5% noise | |
|-----------------------------------|--------------|-----------------------|---------------------|------------------------|---------------------|-----------------------|----------------------|---------------------|---------------------|------------------------|---------------------|---------------|--------------|
| | Size | CD | P2M | CD | P2M | CD | P2M | CD | P2M | CD | P2M | CD | P2M |
| IterativePFN 3DMambaIPF (Ours) | 1000 1000 | 20.55 19.89 | 5.01 4.77 | 30.43 29.95 | 8.43 8.03 | 33.53 32.62 | 10.46 9.92 | 6.05 5.89 | 3.02 2.91 | 8.03 7.55 | 4.36 4.05 | 10.15 9.28 | 5.88 5.31 |
| IterativePFN | 2000 | 20.64 | 5.02 | 30.43 | 8.41 | 33.93 | 10.72 | 6.01 | 2.99 | 7.79 | 4.19 | 10.25 | 5.95 |
| 3DMambaIPF (Ours) | 2000 | 19.98 | 4.81 | 30.05 | 8.14 | 32.73 | 10.04 | 5.92 | 2.92 | 7.52 | 4.05 | 8.98 | 5.13 |

5.3 Comparisons on Small-Scale Datasets

Table 1 presents the results of 3DMambaIPF compared to other baseline methods on PU-Net dataset. Figure 6 illustrates the visualization comparison on PU-Net dataset. Each visualized object contains 50K points with a Gaussian deviation of 2.5% of the bounding sphere radius. 3DMambaIPF outperforms all baseline methods across different resolutions and various levels of noise. Moreover, visual results have shown that 3DMambaIPF exhibits superior filtering performance, particularly with high accuracy in boundary denoising. Specifically, while Pointfilter demonstrates competitive results in terms of CD and P2M metrics, it exhibits geometrically unrealistic deviations in boundary denoising for complex objects (e.g. casting). Compared to other baselines, IterativePFN excels both in terms of metrics and visual presentation, with its only drawback being slightly inferior denoising effects on point cloud boundaries. Conversely, 3DMambaIPF ensures the authenticity of geometric structures and exhibits superior denoising results for boundary sections, while also outperforming in metrics.

5.4 Comparisons on Large-Scale Datasets

The visualization performance of large-scale point clouds is tested on both large-scale synthetic models from the Stanford 3D Scanning Repository and Paris-rue-Madame dataset. In the visualization results of large-scale synthetic datasets, some of the baselines struggle to filter due to the presence of dense and distant noise from the surface. While PointFilter achieves filtering results where each point is close to a clean surface, it lacks significant geometric details and accurate edge structures. It is found that the incorporation of the generative model into PD-Flow results in varied denoising outcomes across different experiments on the same point cloud. Despite potential variations in outcomes, PD-Flow generally falls short in effectively denoising large-scale point clouds, particularly in densely noisy areas where it struggles to achieve significant noise reduction. ScoreDenoise, employing a patch partitioning method, exhibits gaps in results when processing large-scale point clouds. Although IterativePFN addresses this issue with patch-stitching, its performance suffers when handling point cloud edges and densely cluttered point clouds. On the contrary, the inclusion of the Mamba module enhances the processing capabilities of 3DMambaIPF when dealing with dense point clouds. Additionally, the utilization of rendering loss results in remarkable denoising effects specifically on the edges of the point cloud. In the visualization of real-world large-scale dataset (Paris-rue-Madame), when there are no additional noises introduced, all the baseline methods are capable of achieving satisfactory filtering results. 3DMambaIPF outperforms the others in terms of preserving geometric edges.

6 ABLATION STUDY

Ablation experiments are conducted on the influencing factors of 3DMambaIPF, focusing on four aspects: i) loss function, ii) the quantity of rendered images in point rendering, iii) the number of Mamba layers, and iv) patch size. All the ablation experiments are tested on PU-Net dataset with NVIDIA GeForce RTX 3090 GPU. Initially, Table 2 validates the enhancement of the filtering capability of 3DMambaIPF across various levels of noise with the introduction of view loss. Following the previous validation step, we proceed to examine how varying numbers of rendered views affect filtering effectiveness. Table 3 suggests that generally, a greater number of views correlates with stronger denoising ability, with 32 views yielding the best results. However, employing an excessive number of views will decrease the training speed. Subsequently, ablation experiments are carried out on the number of Mamba layers. Table 4 illustrates that the denoising capability is at its peak with 6 Mamba layers. At last, the influence of patch size on denoising capability is examined in Table 5, finding that larger patch sizes are more suitable for larger scenes.

7 CONCLUSION

In this study, we introduce 3DMambaIPF, an iterative point cloud filtering model that utilizes the Mamba module. 3DMambaIPF not only achieves state-of-the-art results on small-scale (PU-Net) dataset, but also demonstrates superior performance on large-scale datasets, indicating its capability to address denoising challenges in extensive scenes, as validated through ablation experiments. Although 3DMambaIPF may encounter reverse-amplification issues on denoising a smooth and clean surface, its performance remains optimal.

REFERENCES

- Marc Alexa, Johannes Behr, Daniel Cohen-Or, Shachar Fleishman, David Levin, and Claudio T Silva. 2001. Point set surfaces. In <u>Proceedings Visualization</u>, 2001. VIS'01. IEEE, 21–29.
- [2] Marc Alexa, Johannes Behr, Daniel Cohen-Or, Shachar Fleishman, David Levin, and Claudio T. Silva. 2003. Computing and rendering point set surfaces. <u>IEEE</u> <u>Transactions on visualization and computer graphics</u> 9, 1 (2003), 3–15.
- [3] Haim Avron, Andrei Sharf, Chen Greif, and Daniel Cohen-Or. 2010. L1-sparse reconstruction of sharp point set surfaces. <u>ACM Transactions on Graphics (TOG)</u> 29, 5 (2010), 1–12.
- [4] Sai Praveen Bangaru, Michael Gharbi, Fujun Luan, Tzu-Mao Li, Kalyan Sunkavalli, Milos Hasan, Sai Bi, Zexiang Xu, Gilbert Bernstein, and Fredo Durand. 2022. Differentiable rendering of neural sdfs through reparameterization. In <u>SIGGRAPH</u> Asia 2022 Conference Papers. 1–9.
- [5] Frédéric Cazals and Marc Pouget. 2005. Estimating differential quantities using polynomial fitting of osculating jets. <u>Computer aided geometric design</u> 22, 2 (2005), 121–146.
- [6] Brian Curless and Marc Levoy. 1996. A volumetric method for building complex models from range images. In Proceedings of the 23rd annual conference on Computer graphics and interactive techniques. 303–312.
- [7] Dasith de Silva Edirimuni, Xuequan Lu, Zhiwen Shao, Gang Li, Antonio Robles-Kelly, and Ying He. 2023. IterativePFN: True iterative point cloud filtering. In Proceedings of the IEEE/CVF Conference on Computer Vision and Pattern Recognition. 13530–13539.
- [8] Ben Fei, Jingyi Xu, Rui Zhang, Qingyuan Zhou, Weidong Yang, and Ying He. 2024.
 3D Gaussian as a New Vision Era: A Survey. arXiv preprint arXiv:2402.07181
 (2024)
- [9] Ben Fei, Weidong Yang, Wen-Ming Chen, Zhijun Li, Yikang Li, Tao Ma, Xing Hu, and Lipeng Ma. 2022. Comprehensive review of deep learning-based 3d point cloud completion processing and analysis. <u>IEEE Transactions on Intelligent</u> Transportation Systems 23, 12 (2022), 22862–22883.
- [10] Ben Fei, Weidong Yang, Liwen Liu, Tianyue Luo, Rui Zhang, Yixuan Li, and Ying He. 2023. Self-supervised learning for pre-training 3d point clouds: A survey. arXiv preprint arXiv:2305.04691 (2023).

- [11] Ben Fei, Rui Zhang, Weidong Yang, Zhijun Li, and Wen-Ming Chen. 2024. Progressive Growth for Point Cloud Completion by Surface-Projection Optimization. IEEE Transactions on Intelligent Vehicles (2024).
- [12] Xianz Gao, Wei Hu, and Zongming Guo. 2018. Graph-based point cloud denoising. In 2018 IEEE Fourth International Conference on Multimedia Big Data (BigMM). IEEE, 1-6.
- [13] Albert Gu and Tri Dao. 2023. Mamba: Linear-time sequence modeling with selective state spaces. arXiv preprint arXiv:2312.00752 (2023).
- [14] Albert Gu, Tri Dao, Stefano Ermon, Atri Rudra, and Christopher Ré. 2020. Hippo: Recurrent memory with optimal polynomial projections. <u>Advances in neural information processing systems</u> 33 (2020), 1474–1487.
- [15] Albert Gu, Karan Goel, and Christopher Ré. 2021. Efficiently modeling long sequences with structured state spaces. arXiv preprint arXiv:2111.00396 (2021).
- [16] Albert Gu, Isys Johnson, Karan Goel, Khaled Saab, Tri Dao, Atri Rudra, and Christopher Ré. 2021. Combining recurrent, convolutional, and continuous-time models with linear state space layers. <u>Advances in neural information processing systems</u> 34 (2021), 572–585.
- [17] Paul Guerrero, Yanir Kleiman, Maks Ovsjanikov, and Niloy J Mitra. 2018. Pcpnet learning local shape properties from raw point clouds. In <u>Computer graphics</u> forum, Vol. 37. Wiley Online Library, 75–85.
- [18] Wei He, Kai Han, Yehui Tang, Chengcheng Wang, Yujie Yang, Tianyu Guo, and Yunhe Wang. 2024. DenseMamba: State Space Models with Dense Hidden Connection for Efficient Large Language Models. arXiv preprint arXiv:2403.00818 (2024).
- [19] Pedro Hermosilla, Tobias Ritschel, Pere-Pau Vázquez, Àlvar Vinacua, and Timo Ropinski. 2018. Monte carlo convolution for learning on non-uniformly sampled point clouds. ACM Transactions on Graphics (TOG) 37, 6 (2018), 1–12.
- [20] Wei Hu, Xiang Gao, Gene Cheung, and Zongming Guo. 2020. Feature graph learning for 3D point cloud denoising. <u>IEEE Transactions on Signal Processing</u> 68 (2020), 2841–2856.
- [21] Wei Hu, Jiahao Pang, Xianming Liu, Dong Tian, Chia-Wen Lin, and Anthony Vetro. 2021. Graph signal processing for geometric data and beyond: Theory and applications. IEEE Transactions on Multimedia 24 (2021), 3961–3977.
- [22] Hui Huang, Shihao Wu, Minglun Gong, Daniel Cohen-Or, Uri Ascher, and Hao Zhang. 2013. Edge-aware point set resampling. <u>ACM transactions on graphics</u> (TOG) 32, 1 (2013), 1–12.
- [23] Jiahao Huang, Liutao Yang, Fanwen Wang, Yinzhe Wu, Yang Nan, Angelica I Aviles-Rivero, Carola-Bibiane Schönlieb, Daoqiang Zhang, and Guang Yang. 2024. MambaMIR: An Arbitrary-Masked Mamba for Joint Medical Image Reconstruction and Uncertainty Estimation. arXiv preprint arXiv:2402.18451 (2024).
- [24] Eldar Insafutdinov and Alexey Dosovitskiy. 2018. Unsupervised learning of shape and pose with differentiable point clouds. <u>Advances in neural information</u> processing systems 31 (2018).
- [25] Bernhard Kerbl, Georgios Kopanas, Thomas Leimkühler, and George Drettakis. 2023. 3d gaussian splatting for real-time radiance field rendering. <u>ACM</u> <u>Transactions on Graphics</u> 42, 4 (2023), 1–14.
- [26] Venkat Krishnamurthy and Marc Levoy. 1996. Fitting smooth surfaces to dense polygon meshes. In Proceedings of the 23rd annual conference on Computer graphics and interactive techniques. 313–324.
- [27] Samuli Laine, Janne Hellsten, Tero Karras, Yeongho Seol, Jaakko Lehtinen, and Timo Aila. 2020. Modular Primitives for High-Performance Differentiable Rendering. ACM Transactions on Graphics 39, 6 (2020).
- [28] Esmeide Leal, German Sanchez-Torres, and John W Branch. 2020. Sparse regularization-based approach for point cloud denoising and sharp features enhancement. Sensors 20, 11 (2020), 3206.
- [29] Dingkang Liang, Xin Zhou, Xinyu Wang, Xingkui Zhu, Wei Xu, Zhikang Zou, Xiaoqing Ye, and Xiang Bai. 2024. PointMamba: A Simple State Space Model for Point Cloud Analysis. arXiv preprint arXiv:2402.10739 (2024).
- [30] Weibin Liao, Yinghao Zhu, Xinyuan Wang, Cehngwei Pan, Yasha Wang, and Liantao Ma. 2024. LightM-UNet: Mamba Assists in Lightweight UNet for Medical Image Segmentation. arXiv preprint arXiv:2403.05246 (2024).
- [31] Yaron Lipman, Daniel Cohen-Or, David Levin, and Hillel Tal-Ezer. 2007. Parameterization-free projection for geometry reconstruction. <u>ACM</u> <u>Transactions on Graphics (ToG)</u> 26, 3 (2007), 22-es.
- [32] Jiuming Liu, Ruiji Yu, Yian Wang, Yu Zheng, Tianchen Deng, Weicai Ye, and Hesheng Wang. 2024. Point Mamba: A Novel Point Cloud Backbone Based on State Space Model with Octree-Based Ordering Strategy. <u>arXiv preprint</u> arXiv:2403.06467 (2024).
- [33] Shichen Liu, Tianye Li, Weikai Chen, and Hao Li. 2019. Soft rasterizer: A differentiable renderer for image-based 3d reasoning. In Proceedings of the IEEE/CVF international conference on computer vision. 7708–7717.
- [34] Chris Lu, Yannick Schroecker, Albert Gu, Emilio Parisotto, Jakob Foerster, Satinder Singh, and Feryal Behbahani. 2024. Structured state space models for incontext reinforcement learning. <u>Advances in Neural Information Processing Systems</u> 36 (2024).
- [35] Shitong Luo and Wei Hu. 2020. Differentiable manifold reconstruction for point cloud denoising. In Proceedings of the 28th ACM international conference on

- multimedia. 1330-1338.
- [36] Shitong Luo and Wei Hu. 2021. Score-based point cloud denoising. In Proceedings of the IEEE/CVF International Conference on Computer Vision. 4583–4592.
- [37] Aihua Mao, Zihui Du, Yu-Hui Wen, Jun Xuan, and Yong-Jin Liu. 2022. Pd-flow: A point cloud denoising framework with normalizing flows. In <u>European Conference on Computer Vision</u>. Springer, 398–415.
- [38] Dereck S Meek and Desmond J Walton. 2000. On surface normal and Gaussian curvature approximations given data sampled from a smooth surface. <u>Computer</u> <u>aided geometric design</u> 17, 6 (2000), 521–543.
- [39] Ben Mildenhall, Pratul P Srinivasan, Matthew Tancik, Jonathan T Barron, Ravi Ramamoorthi, and Ren Ng. 2021. Nerf: Representing scenes as neural radiance fields for view synthesis. Commun. ACM 65, 1 (2021), 99–106.
- [40] Diganta Misra, Jay Gala, and Antonio Orvieto. 2024. On the low-shot transferability of [V]-Mamba. arXiv preprint arXiv:2403.10696 (2024).
- [41] Jan U Müller, Michael Weinmann, and Reinhard Klein. 2022. Unbiased Gradient Estimation for Differentiable Surface Splatting via Poisson Sampling. In <u>European</u> Conference on Computer Vision. Springer, 281–299.
- [42] Leif E Peterson. 2009. K-nearest neighbor. Scholarpedia 4, 2 (2009), 1883.
- [43] Francesca Pistilli, Giulia Fracastoro, Diego Valsesia, and Enrico Magli. 2020. Learning graph-convolutional representations for point cloud denoising. In <u>European</u> conference on computer vision. Springer, 103–118.
- [44] Marie-Julie Rakotosaona, Vittorio La Barbera, Paul Guerrero, Niloy J Mitra, and Maks Ovsjanikov. 2020. Pointcleannet: Learning to denoise and remove outliers from dense point clouds. In <u>Computer graphics forum</u>, Vol. 39. Wiley Online Library, 185–203.
- [45] Yufan Ren, Tong Zhang, Marc Pollefeys, Sabine Süsstrunk, and Fangjinhua Wang. 2023. Volrecon: Volume rendering of signed ray distance functions for generalizable multi-view reconstruction. In <u>Proceedings of the IEEE/CVF Conference on Computer Vision and Pattern Recognition</u>. 16685–16695.
- [46] Oliver Schall, Alexander Belyaev, and H-P Seidel. 2005. Robust filtering of noisy scattered point data. In Proceedings Eurographics/IEEE VGTC Symposium Point-Based Graphics, 2005. IEEE, 71–144.
- [47] Andrés Serna, Beatriz Marcotegui, François Goulette, and Jean-Emmanuel Deschaud. 2014. Paris-rue-Madame database: A 3D mobile laser scanner dataset for benchmarking urban detection, segmentation and classification methods. In 4th international conference on pattern recognition, applications and methods

ICPRAM 2014.

- [48] Yujing Sun, Scott Schaefer, and Wenping Wang. 2015. Denoising point sets via L0 minimization. Computer Aided Geometric Design 35 (2015), 2–15.
- [49] Yogita Thakran and Durga Toshniwal. 2012. Unsupervised outlier detection in streaming data using weighted clustering. In 2012 12th international conference on intelligent systems design and applications (ISDA). IEEE, 947–952.
- [50] Delio Vicini, Sébastien Speierer, and Wenzel Jakob. 2022. Differentiable signed distance function rendering. <u>ACM Transactions on Graphics (TOG)</u> 41, 4 (2022), 1-18.
- [51] Zhichao Yang, Avijit Mitra, Sunjae Kwon, and Hong Yu. 2024. ClinicalMamba: A Generative Clinical Language Model on Longitudinal Clinical Notes. <u>arXiv</u> preprint arXiv:2403.05795 (2024).
- [52] Wang Yifan, Felice Serena, Shihao Wu, Cengiz Öztireli, and Olga Sorkine-Hornung. 2019. Differentiable surface splatting for point-based geometry processing. ACM Transactions on Graphics (TOG) 38, 6 (2019), 1–14.
- [53] Lequan Yu, Xianzhi Li, Chi-Wing Fu, Daniel Cohen-Or, and Pheng-Ann Heng. 2018. Pu-net: Point cloud upsampling network. In <u>Proceedings of the IEEE</u> conference on computer vision and pattern recognition. 2790–2799.
- [54] Yubiao Yue and Zhenzhang Li. 2024. MedMamba: Vision Mamba for Medical Image Classification. arXiv preprint arXiv:2403.03849 (2024).
- [55] Faisal Zaman, Ya Ping Wong, and Boon Yian Ng. 2017. Density-based denoising of point cloud. In 9th International Conference on Robotic, Vision, Signal Processing and Power Applications: Empowering Research and Innovation. Springer, 287–295.
- [56] Dongbo Zhang, Xuequan Lu, Hong Qin, and Ying He. 2020. Pointfilter: Point cloud filtering via encoder-decoder modeling. <u>IEEE Transactions on Visualization and Computer Graphics</u> 27, 3 (2020), 2015–2027.
- [57] Tao Zhang, Xiangtai Li, Haobo Yuan, Shunping Ji, and Shuicheng Yan. 2024. Point Could Mamba: Point Cloud Learning via State Space Model. <u>arXiv preprint</u> arXiv:2403.00762 (2024).
- [58] Han Zhao, Min Zhang, Wei Zhao, Pengxiang Ding, Siteng Huang, and Donglin Wang. 2024. Cobra: Extending Mamba to Multi-Modal Large Language Model for Efficient Inference. arXiv preprint arXiv:2403.14520 (2024).
- [59] Jun Zhou, Wei Jin, Mingjie Wang, Xiuping Liu, Zhiyang Li, and Zhaobin Liu. 2022. Fast and accurate normal estimation for point clouds via patch stitching. Computer-Aided Design 142 (2022), 103121.